Dual Doppler Radar Investigation of the Tropical Convective Boundary Layer

LAURENCE EYMARD AND ALAIN WEILL

CNET/CRPE, Issy-les-Moulineaux, France

(Manuscript received 21 November 1986, in final form 23 September 1987)

ABSTRACT

Radar observations of the convective boundary layer were made during the "COPT81" experiment in May–June 1981 over western Africa. The lower atmosphere was characterized by the interaction between the southerly monsoon and the African easterly jet above it. The mean wind shear between both flows is found to organize convective elements along preferred directions and to transfer energy to the perturbed field (velocity variances, momentum fluxes). However, the convective organization is also the cause of increasing horizontal variance and in some cases of a negative shear stress production. The global behavior of the convective boundary layer in the four observed situations appeared similar to those observed in middle latitudes, but the strong wind shear is an important feature of the layer.

1. Introduction

The use of Doppler radars in the convective boundary layer provides the advantage of simultaneously observing phenomena above a surface of 100 to 200 km^2. Previous works by Hardy and Ottersten (1969), Konrad (1970) and Kuettner (1971) have demonstrated the capability of radar observations for describing convective elements. Frisch et al. (1976), Kropfli and Hildebrand (1980) and Detman and Kropfli (1980) compared radar measurements with data from other instruments. Reinking et al. (1981), Kelly (1982, 1984), Doviak and Berger (1980) studied the convective organization. However, radar data were frequently used for depiction and qualitative description of phenomena, rather than for quantitative determination of boundary layer properties, as by Rabin et al. (1982), Kropfli and Kohn (1978) and Eymard (1984).

In most of the convective layer studies, observations were realized using instrumented towers (Kaimal et al., 1976), tethered balloon (Kitchen and Caughey, 1981; Kitchen et al., 1983) or aircraft (LeMone, 1973; Lenshow et al., 1980; Jensen and Lenshow, 1978 and others), sodar (Weill et al., 1980) or two or more instruments together (Kaimal et al., 1982; Nicholls and LeMone, 1980). In some of these studies, a spatial point of view is considered, but never with simultaneous observations of the convective layer at different locations, as those which can be obtained with Doppler radars.

The present study is concerned with the tropical convective boundary layer, as observed using dual Doppler radar data during the COPT81 experiment. The boundary layer properties are examined at a scale considerably greater than the individual cell scale, contrary to a previous paper by Eymard (1984), in which the observed convective cells were related to cumulus clouds above them. Eymard (1985) determined the origin of the organization of convective cells to be the shear in the horizontal mean wind by applying Asai's model (Asai, 1972.) The goal of this paper is to propose interpretations of four observed events, by relating the first and second order moments of the wind field to the convective organization and the mean profiles.

In the first section, we examine the general features of the observed tropical continental boundary layer and the experimental setting. The second section concerns the effects of shear and convective organization on the horizontal wind components. The vertical velocity properties are detailed in the third section. Then the interpretations of the four cases are discussed.

2. The observations

a. Synoptic situation: the tropical boundary layer during the experiment

The COPT81 (COnvection Profonde Tropicale) experiment was conducted in May and June 1981 at the northern Ivory Coast near the city of Korhogo (Fig. 1). Its main purpose was the observation of thunderstorms and squall-lines as described by Sommeria and Testud (1984), and boundary layer conditions favorable to initiation of deep convection. Strong events frequently occur at the beginning of the rainy season in Africa because of the interaction of the wet southerly monsoon flow and the easterly wind above it (African easterly jet).

Figure 2 presents the synoptic evolution of the zonal and meridional components of the wind during

Corresponding author address: Dr. Laurence Eymard, CNET/CRPE, 38–40 rue de General Leclerc, 92131 Issy-les-Moulineaux, France.

© 1988 American Meteorological Society

Unauthenticated | Downloaded 09/26/22 10:29 AM UTC

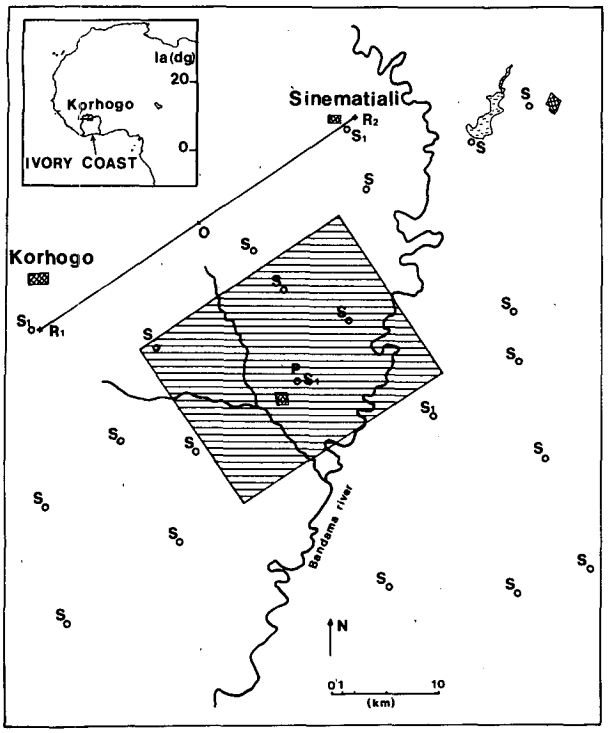

FIG. 1. Map of the experimental area. Radars were located at points R_1 and R_2. The surface meteorological network is indicated by symbols S and S_1, the latter corresponding to flux measuring stations. The sounding station was located near the R_1 radar and the three antennae Doppler sodar was beside R_2. The area of synthetized winds is hatched.

one month of the experiment. Data come from wind soundings performed by EERM (Etablissement d'Etudes et de Recherche de la Météorologie) at least once every day in the experimental area. The monsoon flow extends up to about 1 km, fluctuating in direction between 150° and 240° and with the mean speed 4 m s^{-1}. The easterly wind is roughly constant in direction (90°) but is varying in speed between 10 and 25 m s^{-1} near a height of 3 km. At the transition level between both flows, a shear occurs, essentially in direction up to 1.5 km and in speed at the base of the easterly flow. Both flows interact: when the easterly wind is a maximum (about 20 m s^{-1}), the monsoon blows toward the northwest. However the low altitude wind blows toward the northeast when the easterly wind is lower (12–15 m s^{-1}).

Another important aspect of these flows can be seen in Fig. 3, which shows the mean profiles of virtual potential temperature and relative humidity for three periods during the experiment (13–29 May; 30 May–7 June; 9–18 June). The humidity is very low (minimum 5%–10%) in the easterly wind at the beginning of June whereas it is generally greater than 50% in May and after 8 June. This period during the season of monsoon arrival is characterized by a convective layer top between 1 and 1.5 km located inside the monsoon flow, in the transition layer between both flows or in the easterly wind, depending on the convective development.

b. The boundary layer experiment and radar methodology

The instrument location is indicated in Fig. 1. The experimental site was close to the city of Korhogo, at the northern Ivory Coast. The two Doppler radars (RONSARD system, Nutten et al., 1979) were located at points R_1 and R_2. These C-band radars were operating following the coplane methodology (simultaneous exploration in a series of planes tilted about an axis along the radar baseline, developed by Miller and Strauch, 1974). Above the hatched rectangle, chaff was released from an aircraft at height 600 m. At point P in the radar domain, a full-sky camera took pictures during every experiment. The other instruments consisted of a surface meteorological network noted by S, a radiosonde station near the R_1 radar and a three antennae Doppler sodar beside R_2. Further details about the experimental setting can be found in Eymard (1984) concerning the boundary layer and in Sommeria and Testud (1984) concerning the entire experiment.

The times and durations of the observations studied in this paper (all times UTC) are listed in Table 1 for radars, sodar and soundings. Since boundary layer study was not the principal object of the COPT81 experiment, only four observations each of one hour duration could be successfully performed on 24, 26 May and 6 June (noted a, b, c, d in the following, as indicated in Table 1).

Using the data processing developed by Testud and Chong (1983), Chong et al. (1983) and Chong and Testud (1983), the three components of the wind field were obtained in a volume of horizontal base about 12 × 12 km^2 and 1 to 1.8 km in height, with grid point separations 300 m in the horizontal and 100 m in the vertical. The accuracy was estimated to be 0.1–0.15 m s^{-1} for horizontal components and 0.2–0.25 m s^{-1} for the vertical component (see Eymard, 1984, for a more complete description of the data processing).

In each experiment, 6 to 10 volume analyses (scans) were examined, providing a detailed description of the boundary layer in space and in time (the scan duration was 3.5 min). In this study our interest is the mean behavior of the convective layer, so we examine mean vertical profiles calculated within the entire volume. However, the grid separation prevents one from studying phenomena on a scale smaller than 1 km, because of the small scale filtering over three grid points.

c. Mean characteristics of the observed cases

In the four cases, wind profiles were obtained using the mean winds deduced from radar data and wind soundings. They are plotted in Fig. 4 and potential temperature, virtual potential temperature and hu-

Unauthenticated | Downloaded 09/26/22 10:29 AM UTC

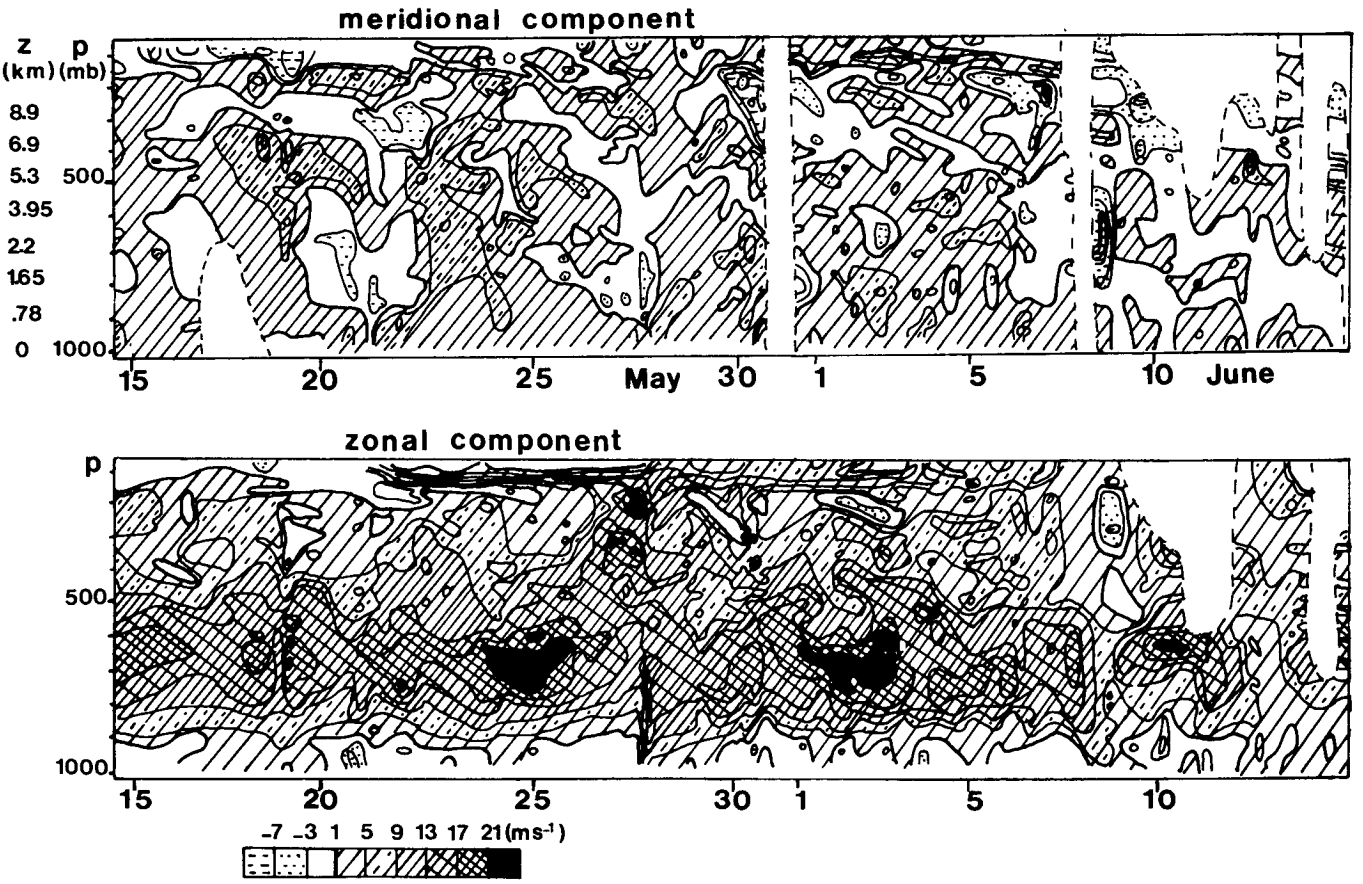

FIG. 2. Synoptic meridional (positive toward the N) and zonal (positive toward the W) components of the wind from wind soundings made at the experimental site during the "COPT81" experiment between 15 May and 15 June 1981.

midity profiles are shown in Fig. 5. The three days present the following characteristics:

• *24 May:* a strong easterly wind is observed (24 m s^{-1} at height 3 km), with a vertical shear of about 0.015 s^{-1} and the humidity is high (60%). Although high humidity favors convective development, no deep convection event was observed on 24 May. The boundary layer is identifiable inside the entire monsoon layer until midday and its top reaches 1.2–1.3 km during the afternoon. A few small cumulus, traveling toward the NNW with the monsoon flow and based near 1

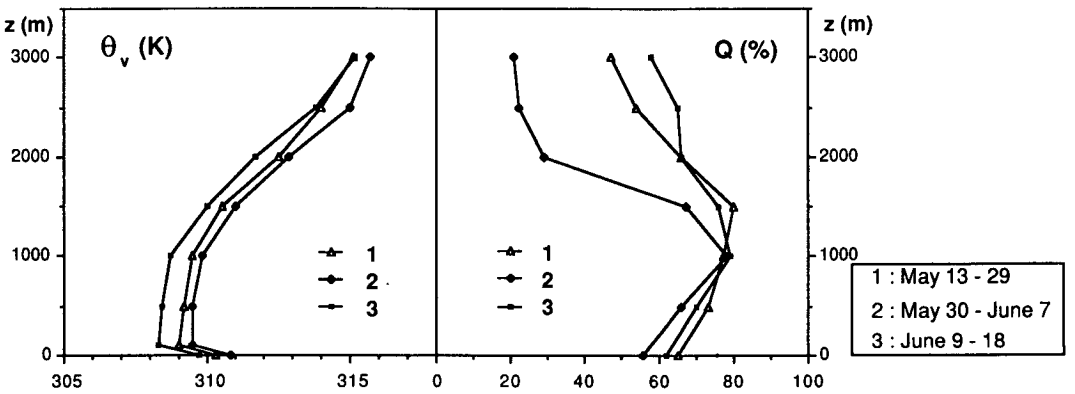

FIG. 3. Mean profiles of virtual potential temperature and relative humidity in the low atmosphere during the COPT81 experiment. Using soundings in fair weather conditions, three periods could be distinguished and characterized by their humidity feature. They are noted 1, 2, 3 on the figure.

Unauthenticated | Downloaded 09/26/22 10:29 AM UTC

TABLE 1. Times and durations of observations using the principal instruments involved in this study: the radars, the sodar and soundings of wind and temperature.

Date	Radars (all UTC)	Sodar (all UTC)	Soundings (all UTC)
24 May (a)	1015–1120	1000–1200	0820 and 1136
(b)	1540–1640	1400–1600	1451 and 1750
26 May (c)	1450–1610	1430–1630	1412 and 1750
6 June (d)	1550–1625	/	1438 and 1717

km, were observed between 10:00 and 12:00. Between 15:00 and 15:50 many clouds were found to travel toward the WNW at altitudes between 1.6 and 2.2 km and then disappeared.

- *Afternoon 26 May:* the easterly wind is relatively weak (12 m s^{-1}) and the monsoon is toward the northeast (the shear is about 0.0075 s^{-1} above the boundary layer). Because of a saturated layer between 500 m and 1.1 km, the sky contained stratus and very few fair weather small cumulus could be seen.
- *Afternoon 6 June:* there is a strong directional shear between the monsoon blowing toward the N, and the easterly wind blowing toward the SW at height 1.5 km. This day takes place in the second period, characterized by a very dry layer (10%–20% relative humidity) above the convective layer. Because of the dry layer, local deep convection was hindered. However, an advected squall-line was observed during the night. The boundary layer extended within the monsoon layer and the base of the easterly flow, and shallow cumulus formed above the inversion layer, traveling toward the NW.

The boundary layer tops determined from radiosonde temperature data, and surface characteristics of the three days from the surface station near R_1 are listed in Table 2. During the morning, the Monin-Obukhov length is of the order of −15, −20 m and decreases during the afternoon, reaching −35 m in cases c and d but −60 m in case b. The surface stress u_* is similar during the entire experiment, of the order of 0.3 m s^{-1}. Except in case a, the experiments were performed in lower flux situations (the sensible heat flux was about 100 W m^{-2} in cases b, c and d compared to 180 W m^{-2} in case a).

Another indication about the convective development may be obtained by looking at the vertical extension of chaff diffusion, since it is related to turbulence associated with convective elements. In case a, chaff diffused through the entire boundary layer without crossing the capping inversion; in case c, chaff reached 900–1000 m, and in cases b and d, chaff reached the cloud base (about 1.7 km) locally, crossing the mean inversion level.

The mean characteristics of the four cases are therefore the following: case a (24 May morning) was a situation of rising inversion capping the convective layer; case c (26 May) was a case of weakly developed convection, whereas cases b (24 May afternoon) and d (6 June) contained well-developed convection associated with cumulus clouds.

3. Effects of shear and convective organization

a. Spatial convective organization

The organization of convective elements is an important aspect of the boundary layer dynamics because the energy carried by cells also presents preferred scales and directions. For example, LeMone (1976) showed that small turbulence can be modulated by two-dimensional rolls without any coupling between roll and turbulence scales. Moreover, such an organization is the effect of the interaction between the mean flow and the convective layer. The resulting properties of the turbulent flow have to be interpreted in relation to both the mean flow and the organized convection, or "secondary flow," following Brown (1972) and Brown (1980).

Eymard (1985) studied the spatial organization of convective elements in the four cases using two-dimensional spectral analysis of the vertical velocity field at every height level of every scan. Mean spectral diagrams were determined in each case (Fig. 6), in order to characterize the preferred scales and directions. On this figure, each point corresponds to the center of a peak observed at several levels of one scan. If peaks are clustered in small areas, it means that an organi-

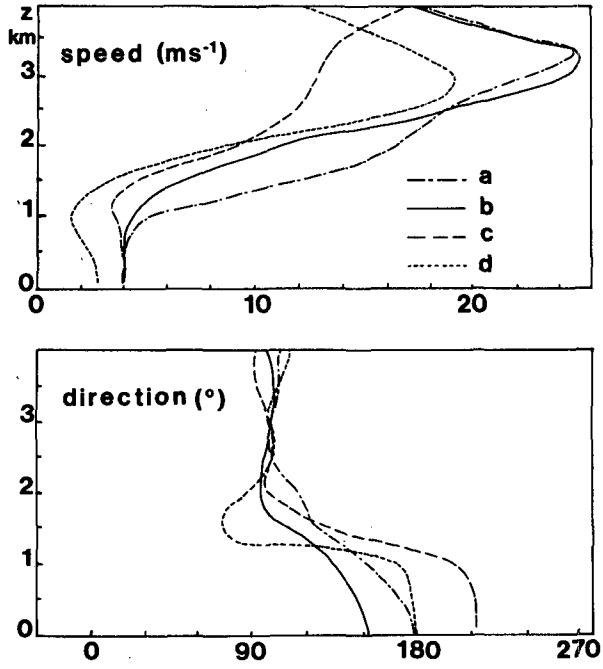

FIG. 4. Mean wind profiles during the four experiments. They are constructed using wind-soundings and radar winds for the lower part. The direction of a south wind is 180°.

Unauthenticated | Downloaded 09/26/22 10:29 AM UTC

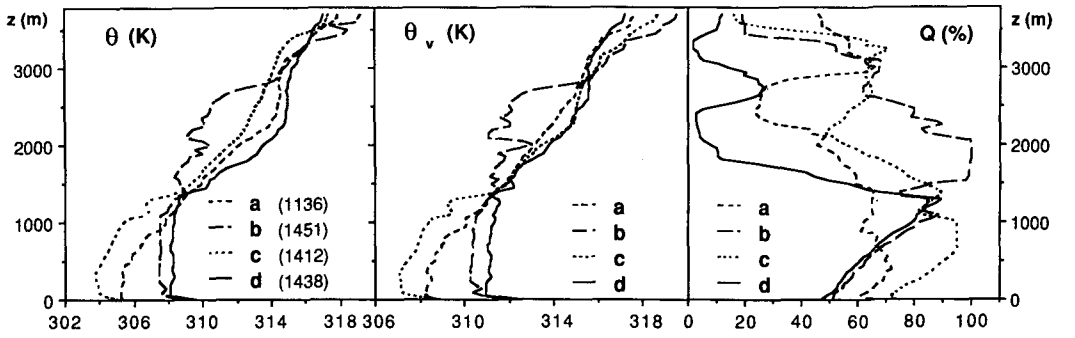

FIG. 5. Potential temperature, virtual potential temperature and humidity profiles during the four experiments.

zation exists in bands perpendicular to the mean wavenumber vector. The analysis method was described by Eymard and Weill (1982).

Among the four cases, there is no case of homogeneous convection, but two of them (a and d) are much more organized than the others (preponderant modes are circled in Fig. 6). Applying Asai's model with the actual wind and temperature profiles, the organization was found to correlate with the wind shear inside the well-mixed layer or at the base of the capping stable layer. The preferred directions of alignment are parallel or transverse to the shear vector depending on the thermal stratification. The four cases may be divided into two groups.

1) Cases a and c are essentially characterized by transverse modes related to the stable layer in the second half of the boundary layer or at the top of the mixed layer. However, case c is poorly organized because of the weak shear and also presents a small longitudinal mode;

2) Cases b and d present longitudinal modes, but a transverse mode is also found in case b. Nevertheless, in case b, both modes are poorly defined in direction. Using several simulations from Asai's model, this difference was found to be due to the shear and the thermal stratification, stronger in case d.

b. *Horizontal velocity variances*

To examine the effects of the convective organization on the turbulence properties, we calculated the mean profiles of horizontal velocity variances in each case with respect to the preferred directions of alignment defined in the previous study. They are plotted in Fig. 7, normalized using the surface convective velocity w_* (see Table 2). In each case the direction is chosen as the one with the maximum spectral energy mode, also corresponding to the longest wavelength in cases a, c and d (in case b, both modes are perpendicular to each other, and we chose the one which was well simulated using the model). The U component is thus chosen parallel to the wavenumber vector, and the V component is parallel to the alignment direction.

All the variances are in the range 0.15–$0.5w_*^2$ except $\overline{U'^2}$ in case d, which is about $0.85w_*^2$ below 1.3 km. These values agree with other measurements by Caughey and Palmer (1979) and Lenshow et al. (1980) despite of the small scale filtering (under 1 km due to data processing). However these authors found variances nearly constant or weakly decreasing with height contrary to our observations, because of the strong wind shear.

The effects of the organization may be depicted in cases a and d, since the U-variances are greater than

TABLE 2. Boundary layer tops Z_i and mean surface layer characteristics in the morning (1030–1200) and afternoon (1430–1700). T_s: temperature near the surface. F_s: sensible heat flux at the surface. w_*: convective velocity. L: Monin-Obukhov length. u_*: friction velocity. (All times UTC.)

	24 May		26 May		6 June	
	Morning (a)	Afternoon (b)	Morning	Afternoon (c)	Morning	Afternoon (d)
Zi (m)	900	1200	≈700	1100		1600
T_s (°C)	31	33	30	31	32.5	33
F_s (W m^{-2})	190	100	135	90	130	80
w_* (m s^{-1})	1.4	1.3	—	1.25	—	1.5
L (m)	−21	−61	−15	−32	−15	−36
u_* (m s^{-1})	0.32	0.35	0.26	0.31	0.25	0.27

Unauthenticated | Downloaded 09/26/22 10:29 AM UTC

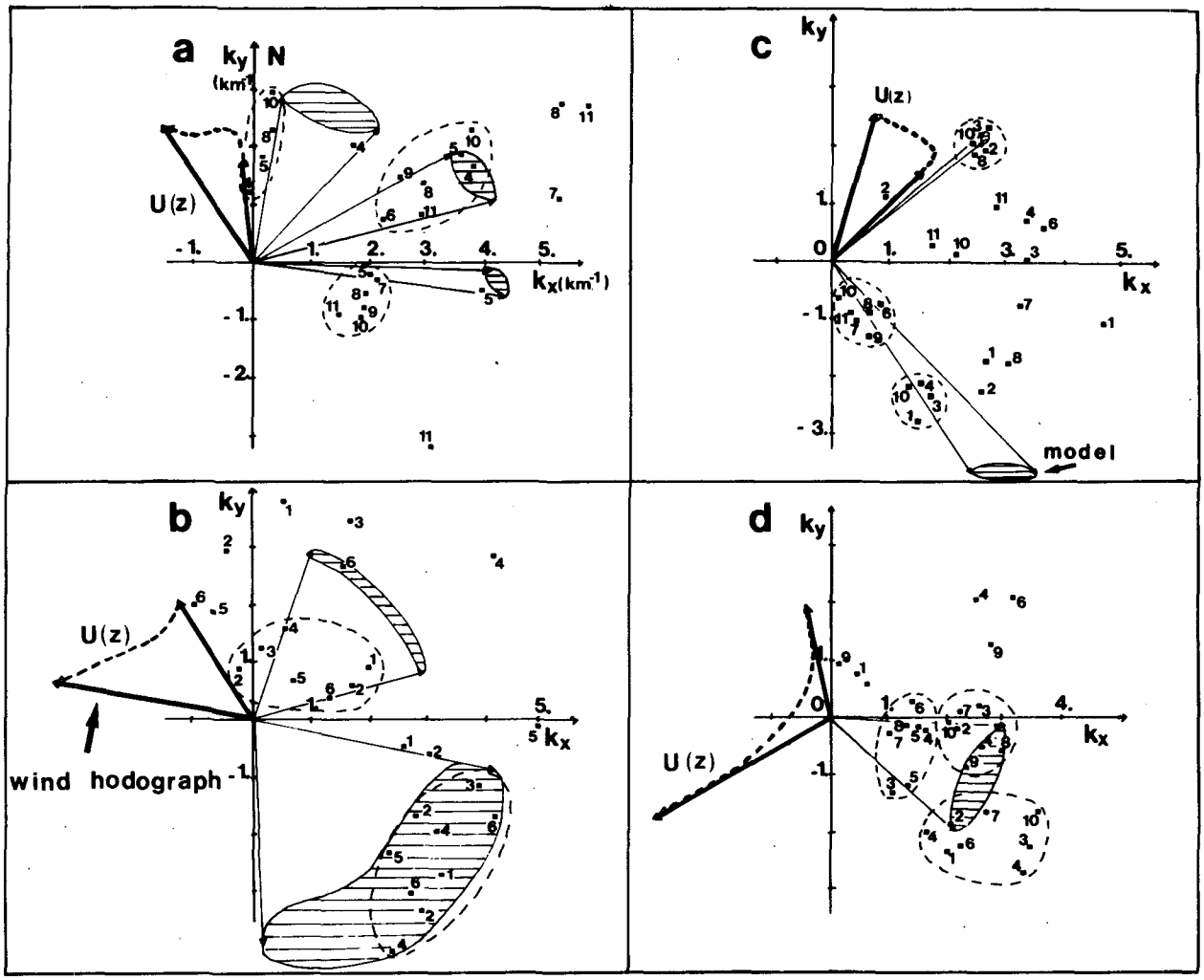

FIG. 6. Spatial organization of the convective elements. Predominant observed modes from every scan (noted with the different numbers) are encircled with a dashed line. Results of the model are superimposed, the hatched areas showing simulated preferred modes.

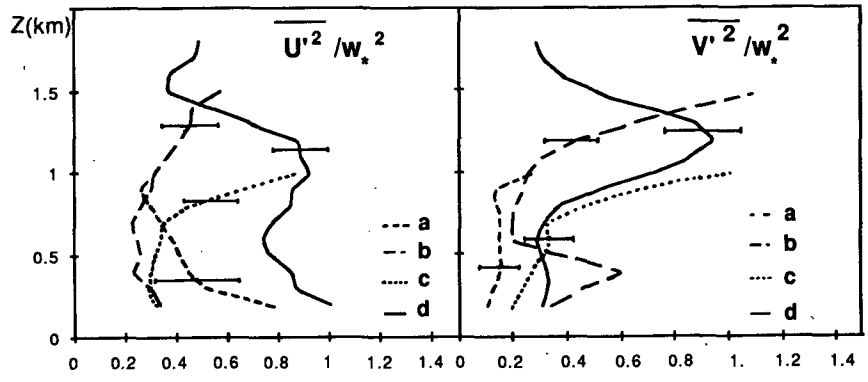

FIG. 7. Mean variances of the horizontal wind components, with respect to the direction of the preferred mode of organization: U is the component parallel to the wavenumber vector, and V is the alongband component. For each case, values are averaged within the entire experiment duration and normalized using the convective velocity w_*. The mean standard deviation for each profile (all levels) is plotted, also normalized using w_*.

Unauthenticated | Downloaded 09/26/22 10:29 AM UTC

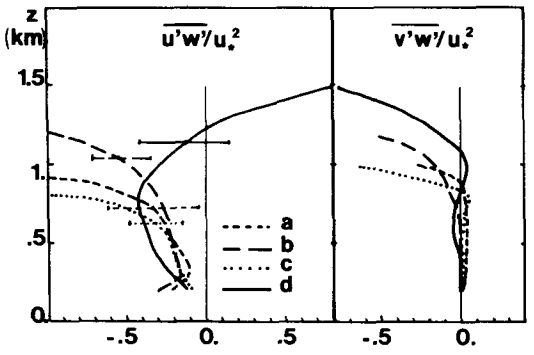

FIG. 8. Mean profiles of momentum flux components, calculated with respect to the monsoon wind direction (u and v are longitudinal and transverse components). Fluxes are normalized using the surface stress u_*^2 measured near the R_1 radar. The mean standard deviations are indicated, also normalized using u_*^2.

the V-variances (difference $U - V$ is about $0.5w_*^2$ in case d and mean difference $0.35w_*^2$ in case a). In case c, U and V variances are very similar, and close to each other below height 1 km in case b. These different behaviors are due to the well-defined modes in cases a and d, in contrast to the others and also because perpendicular peaks were observed both in cases b and c. Such a great variance in the direction transverse to the alignments was also observed by LeMone (1976), who found a higher energy at the roll scale.

Superimposed on this organization is the energy transfer from the mean shear to the turbulent flow (at the scales resolved by the radars). Turner (1973) and Wyngaard (1981) showed that this is a cause of increasing variance, the energy being distributed from the component in the shear direction to the other components through the pressure term. This can be observed in cases b and c on both components in the upper part of the profiles, and on the V component in case d at the maximum shear level (component parallel to the shear direction at 1200 m as shown in Fig. 6).

Thus, the examination of the convective flow in directions related to the main organization shows the mean turbulent properties of the layer modified by the "secondary flow," as described by LeMone (1976). We will now examine the shear stress production.

c. *Momentum fluxes and shear stress production*

From radar velocity data, spatial momentum fluxes can be directly derived using two-dimensional cross-correlation of horizontal and vertical component fields. Because of the small-scale filtering, the results are not representative of the small scale turbulent fluxes. This scale is important, since most of the energy is found between 100 m and several kilometers (Kaimal et al., 1976). Nevertheless, these calculations provide the momentum transports associated with the organized flow and to large eddies (kilometer scale) when considering the entire radar domain.

At the radar domain scale, two-dimensional cross-correlations of velocity perturbations were calculated within about 1500 grid points, yielding a flux accuracy of the order of 5×10^{-3} m^2 s^{-2}. Calculating the mean shear by second-order polynomial differentiation of the averaged horizontal wind speed, the shear production can be deduced from momentum fluxes with an accuracy of about 2×10^{-5} m^2 s^{-3}. Fluxes are plotted in Fig. 8 and shear production in Fig. 9, all normalized using the surface stress u_* (see Table 2). The wind components are referred to the mean monsoon wind at height 0.2–0.5 km.

As also observed by Pennell and LeMone (1974), the transverse fluxes $\overline{v'w'}$ are very weak in the mixed layer, when compared to $\overline{u'w'}$ values (difference of about $0.2u_*^2$, as seen in Fig. 8). Because of the shear in the second half of the convective layer, no systematic decrease with height is observed above $0.5Z_i$, contrary to results obtained by Pennell and LeMone (1974), Rabin et al. (1982) and Kaimal et al. (1976). All stress values are in the same range 0.2–$0.3u_*^2$ (u component) and increase near the inversion level in absolute value, reaching at least u_*^2. However, in cases a, b and c, fluxes $\overline{u'w'}$ and $\overline{v'w'}$ have a similar behavior at high level, being negative. Because of the choice of the monsoon wind direction as the u-axis, $\overline{u'w'}$ is positive in case d above 1.3 km (the projection of the shear vector is negative contrary to the other cases as seen in the wind hodographs in Fig. 6).

The shear-stress production (Fig. 9) is close to zero in the mixed layer in cases a and c. It is slightly negative (-0.2×10^{-4} m^2 s^{-3}) in case b, negative also in case c near the inversion layer and strongly negative near 0.8–1 km in case d (-10^{-4} m^2 s^{-3}). Eymard (1984) calculated shear stress production for the last case inside boxes of horizontal scale 3.5–4 km, and found a positive value of about 0.5×10^{-4} m^2 s^{-3} at 1 km (right part of Fig. 9). To analyse the cause of this difference,

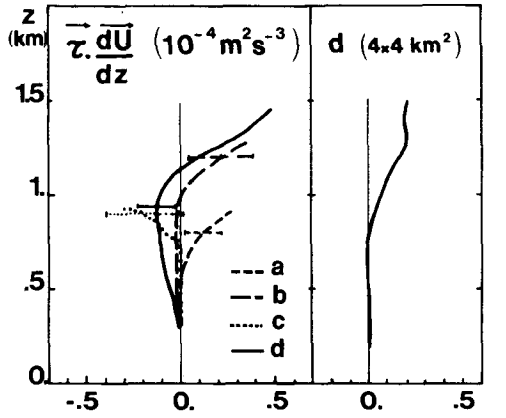

FIG. 9. Left panel: Mean shear stress production profiles $\tau dU/dz$ and mean standard deviations in the four cases. Right panel: mean shear stress production profile computed within boxes of horizontal size 3.5–4 km in case d (Eymard, 1984).

Unauthenticated | Downloaded 09/26/22 10:29 AM UTC

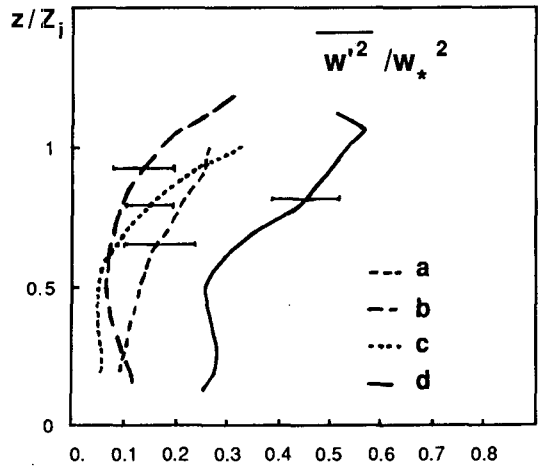

FIG. 10. Mean vertical variance profiles and standard deviations normalized using w_*.

we may follow LeMone (1976): all perturbations are decomposed into a "roll" term, a term of kilometer-scale turbulence and a small scale turbulence term. For example, $u = u_r + u'' + u'$ in this order. She also made the hypothesis that all correlations between terms of different kind are zero ($\overline{u_r v'} = \overline{u'v''} = \overline{u''v_r} = 0$ and similarly for the others). Using radars the small scale turbulence is filtered out, so the shear stress production here may be written as

$$(\overline{u_r w_r} dU/dz + \overline{v_r w_r} dV/dz) + (\overline{u''w''} dU/dz + \overline{v''w''} dV/dz).$$

The first term in parentheses is the production associated with the rolls, and the second one is the kilometer-scale turbulence production. This last term essentially was calculated in Eymard (1984) whereas calculations within the entire domain include the roll production as well (several rolls are observed). Comparing the profiles obtained in both cases shows that there is no shear production in the mixed layer at the turbulence scale, therefore the negative value observed on the other profile between 0.4 and 1.1 km is related to the roll properties. Similarly, Pennell and LeMone (1974), Rabin et al. (1982) and Lenshow et al. (1980) found negative values in case of rolls. This was interpreted as energy transferred back to the mean flow. However, the globally positive production within the entire convective layer suggests that a part of roll energy could be transferred vertically through the transport terms (in the kinetic energy budget).

In the shear layer near the inversion height the production is positive on both profiles in case d (values are in the same range) as well as in cases a and b (Fig. 9), indicating that the shear contributes to the eddy maintenance, in agreement with the greater variances at these heights. However, the error in these computations also increases because of the smaller number of data points near the layer top.

4. Vertical velocity variances and spectra

a. *Variances*

For a well-mixed layer the vertical velocity variance profile has been described by Kaimal et al. (1976), Caughey and Palmer (1979), Lenshow et al. (1980). Following these authors, the variance increases from the surface layer up to $0.4Z_i$ where it reaches 0.4–$0.5w_*^2$ and above more or less decreases with height. Near the inversion level, its value depends on several parameters such as the cloudiness or shear.

Figure 10 shows the mean vertical velocity variances in the four cases, normalized using w_*. In case d the variance is about $0.25w_*^2$ in the mixed layer, and it is in the range 0.03–$0.1w_*^2$ in the other cases. Above $0.5Z_i$, all variances increase with height because of shear production, as seen in the previous section, and also because of entrainment, at least in case d. In the mixed layer, the radar variances are therefore much smaller in cases a, b and c than in case d. All are smaller than those described by the previously cited authors, because of the small-scale filtering below 1 km.

b. *Spectra*

To analyze the causes of the small variances in cases a, b and c, vertical velocity spectra have to be examined.

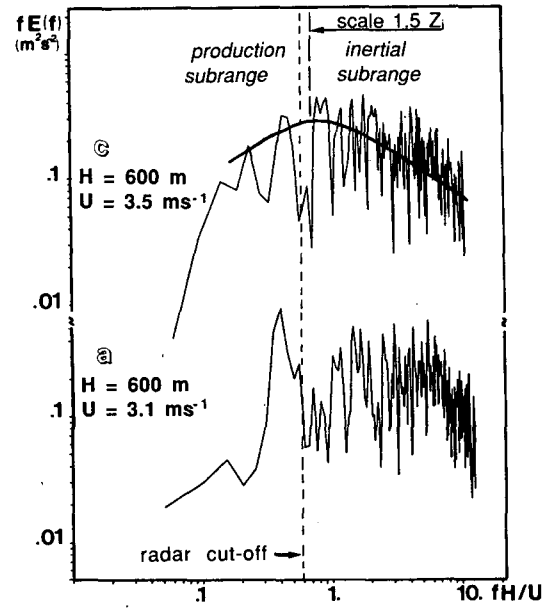

FIG. 11. Vertical velocity spectra from sodar data in cases a and c. The spectral energy is plotted as a function of the normalized frequency fH/U, where H is the top of the neutral layer and U is the mean wind speed. A typical spectrum (from Kaimal et al., 1976) is superimposed to the sodar spectrum in case c (thick line).

Unauthenticated | Downloaded 09/26/22 10:29 AM UTC

Kaimal et al. (1976) established the typical shape of spectra when plotted in function of the normalized wavenumber kZ_i (Fig. 11): at the end of the production subrange, the energy is maximum near 0.67 (wavelength $1.5Z_i$) and decreases in the inertial subrange following a $k^{-5/3}$ law. This behavior was confirmed by Kaimal et al. (1982) above uneven terrain and further generalized by Olesen et al. (1984). Thus, depending on the inversion height, the smallest scale analysed by radars ($\geq$1 km) is in the inertial subrange or in the production subrange. Consequently, the radar velocity variances should be greater in the first case than in the latter one. However, as in the four observed situations, Z_i is equal to or a little greater than 1 km, the measured variances should have been close to each other.

To study the spectral behavior of the vertical velocity in the well-mixed layer in cases a, b and c we used sodar data (the sodar was inoperable on 6 June). Although these records are only available in the lowest 200 m of the atmosphere, they allow one to describe a part of the mixed layer (0.1 to $0.2Z_i$) between scales of several kilometers and small scales (<100 m) in the inertial subrange (the time resolution is 8 s).

Figure 11 is a plot of vertical velocity spectral energy versus the nondimensional frequency fH/U (H characteristic height, U sodar mean wind) in cases a and c. The height 0.6 km, chosen as H, corresponds to the base of the stable layer observed on potential temperature profiles in both cases (Fig. 4). Superimposed on the sodar spectrum in case c is a typical energy spectrum shape, following Kaimal et al. (1976). In both cases, the maximum energy is found around scale $1.5H$. The actual well-mixed layer extends only in the lower 600 m of the atmosphere and hence the radar cutoff (dashed vertical line in Fig. 11) is located inside the production subrange. In cases a and c, radar observations only concern kilometer-scale eddies which rise up to the inversion near 1 km, carrying enough turbulence to diffuse chaff in the entire layer. Their scale ($1.5Z_i$ or more), determined using two-dimensional spectral analysis (Fig. 6), is related to this height.

In case b the vertical velocity variance (Fig. 10) was weak and decreased with time, though the inversion level was at 1.25 km in the mean, capping a neutral layer. Nevertheless, in the sodar spectrum (Fig. 12) the energy does not decrease at wavenumbers greater than 0.67 ($1.5Z_i$) in the "inertial" subrange. It is in the mean larger than the spectral energy in the "production" subrange. This very low energy at kilometer scale is also observed on radar one dimensional spectra computed along the wind direction (a spectrum is superimposed to the sodar one in Fig. 12). It is the cause of the very small variance, although the radar cutoff scale is smaller than $1.5Z_i$.

In case d, sodar data were lacking and it was not possible to examine the spectral behavior in this case. However, the vertical velocity variance is large enough to suggest that the principal convective scales are observed by radars (Z_i = 1.5–1.6 km, so the radar cutoff is in the inertial subrange).

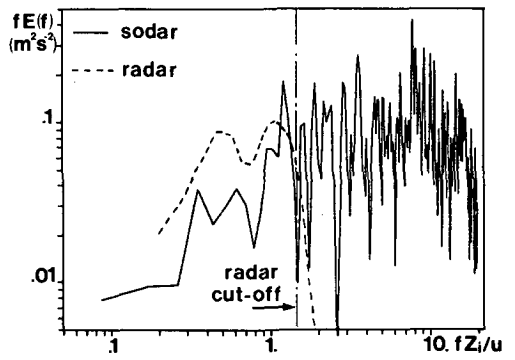

FIG. 12. Sodar and radar mean vertical velocity spectra in the wind direction in case b. The normalized frequency is calculated using the mean sodar wind and the inversion height Z_i (1200 m).

c. *Interpretation of case b (afternoon 24 May)*

Figure 13 presents a comparison between cross sections of the wind field along the radar axis direction for cases b (bottom) and d (top) at 1600. In case d vertical movements are strong, associated with convective cells, and reach or cross the saturation level at 1.6 km: the entire layer is convective. On the contrary, in case b, convective elements are weak, and none of them cross the saturation level, whereas the easterly wind above it presents large oscillations.

Observing these oscillations on several cross sections suggested an application of Stull's model (1976) concerning waves generated by convective cells. The condition for waves to develop are the following: the temperature jump $\Delta\theta$ at the inversion level must be small, as well as the Brunt–Väisälä frequency N just above the interfacial layer (inversion base), but the Richardson number Ri must be greater than its critical value 0.25. If the Brunt–Väisälä frequency of the free atmosphere N_{SA} is smaller than N, internal waves generated above the inversion can propagate upward, limiting convective entrainment. They dissipate a significant part of convective energy when $\Delta\theta/w_0$ is small enough (w_0 being the upward velocity of the convective perturbation). In Table 3, these parameters are listed for cases b and d, showing that the conditions for waves to exist are verified in case b but not in case d, because of the larger temperature step at the inversion and the stronger stability above.

Applying Stull's model to case b, we calculated the expected wave characteristics using radar data and temperature soundings. These calculations are only approximate because the soundings were performed earlier and later than the radars observations and because the mean wave velocity perturbations were deduced from radar velocity variances (which only take into account scales between one and several kilometers). The horizontal wavelength was determined to be

Unauthenticated | Downloaded 09/26/22 10:29 AM UTC

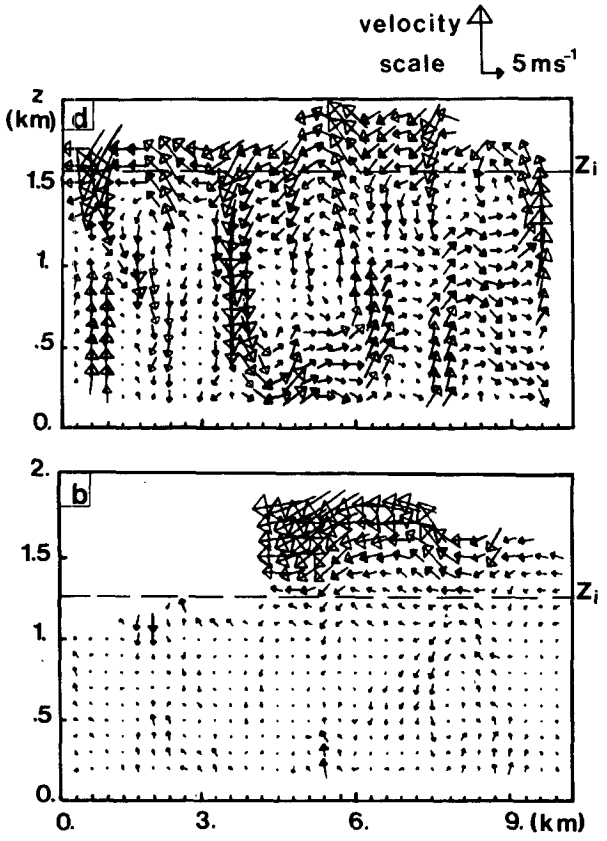

FIG. 13. Vertical cross sections of the wind field in cases d (6 June) in the upper part, and b (Afternoon 24 May) at the bottom. The vertical planes are parallel to the radar baseline, corresponding to the wind direction at height 2 km in case d, and to a direction different from the easterly wind by an angle of 30° in case b. The inversion height (Z_i) is indicated in both cases. The vertical scales of distance and speed are multiplied by a factor 3 to improve the legibility.

about 3 km, corresponding to a propagation toward the northwest, using the two-dimensional vertical velocity spectra between 1530 and 1600 above 1.2 km. Following Stull's wave perturbation formulas relating the velocity perturbations to the wavenumbers, we deduced the vertical wavelength (3300 m) using the relationship $\overline{u'} = (km\overline{w'})/k_h^2$ (k horizontal wavenumber component in the u direction, m vertical wavenumber and k_h horizontal wavenumber), then the intrinsic frequency ($\omega_i = 0.006\ s^{-1}$) and the path ray ($\xi = 47°$). These characteristies are in agreement with a vertical propagation since ω_i is not greater than N_{SA} and ξ is large enough to avoid reflection.

We also estimated the mean wave displacement ($\eta = \overline{w'}/\omega_i = 130$ m) related to the maximum overshoot d through the wave energy equation, yielding $d = 185$ m, and the wave group velocity $w_g = 1.4\ m\ s^{-1}$. This group velocity means that there is a significant energy transport by waves, corresponding to an energy loss by initial convective perturbations of the order of 20%, using Fig. 5 in Stull's paper (percentage of energy loss plotted as a function of $\Delta\theta/w_0$ and γ the temperature gradient in the stable layer).

Thus this theory may explain the anomalously small vertical energy observed in the production subrange at every level (sodar and radar spectra) and its decrease with time. Because of this energy loss, the large convective elements are inhibited and are weakly organized.

5. Summary and conclusion

We presented a study of four cases of a tropical convective boundary layer using Doppler radar data acquired during the COPT81 experiment. The lower atmosphere during May and June in the northern Ivory Coast was found to be characterized by the interaction of the southerly wet monsoon flow with the African easterly jet above it through a speed and directional wind shear.

In a previous paper (Eymard, 1985) the shear was shown to organize the large convective elements in bands parallel (cases b and d) or transverse (cases a and c) to the shear direction. This energy input from the mean flow was studied here by calculating velocity variances, momentum fluxes and shear stress production. There are greater variances observed in the component transverse to the band in cases a and d (well-organized convection) than in the parallel component. The altitudes with large shear are found also to correlate with greater variances in the four cases. Momentum fluxes are greater in the mean wind direction inside the mixed layer but both components increase in the shear layer with a corresponding positive production obtained at the same height in cases a, b and d. However, a negative production appears in the shear layer in case c and in the mixed layer in case b and particularly in case d. In the last case, rolls are responsible for this negative value. This suggests an energy transfer in the vertical, since the mean production within the entire layer is positive.

The four cases were separately interpreted. Cases a and c were situations with weak convective energy be-

TABLE 3. Conditions for internal waves to exist and propagate upward above the convective boundary layer, following Stull (1976): N_{SA} is the Brunt–Väisälä frequency of the free atmosphere, N the Brunt–Väisälä frequency of the layer just above the interfacial layer (inversion base) which must be as small as possible (typically 0.01 is the order of magnitude in many observed situations), Ri the Richardson number in the same layer (stable layer), w_0 the mean velocity of penetrative updrafts and $\Delta\theta$ the temperature jump at the inversion, which must be respectively large and small enough in order to verify the condition $\Delta\theta/w_0 < 0.5$.

	N_{SA} (s^{-1})	N (s^{-1})	Ri	w_0 ($m\ s^{-1}$)	$\Delta\theta$ (°C)	$\Delta\theta/w_0$ (°C s m^{-1})
Stull	small $<N$	small (≤ 0.01)	large >0.25	large	small	<0.5
24 May	0.006	0.0079	1.	0.42	0.2	0.48
6 June	0.009	0.012	0.65	0.6	1.1	1.8

Unauthenticated | Downloaded 09/26/22 10:29 AM UTC

cause of a stable layer in the upper half of the boundary layer. In case b, the small vertical velocity variance is due to internal gravity waves in the stable layer above the inversion, generated by the strongest cells which propagate upward and dissipate an important part of the convective energy (following Stull, 1976). Finally case d is the only case of well-developed convection through the entire boundary layer, and in which the convective organization has the most important effects on variances and momentum production.

Thus, this continental tropical convective boundary layer presents similar properties to those of a middle latitude convective boundary layer. The radiative inversion rises when convection develops in the morning, and convective elements have sizes related to its height. This was also observed by Nicholls and LeMone (1980) in a tropical marine convective boundary layer during GATE.

However, in the middle latitude case, the mean conditions often change from one day to another. A strong shear at the top of the boundary layer can occur for example in the case of dynamic instability generated rolls containing convective forcing (Brown, 1972, 1980), in frontal systems with two superposed synoptic flows interacting in the boundary layer or in orographically induced circulations. On the contrary, in the tropical boundary layer studied in this paper, the Coriolis force is negligible but the strong shear between the monsoon and the easterly wind is a permanent feature during the months of May and June. Its effects are important on the boundary layer properties (convective organization, velocity variances and momentum flux modifications) and the associated dynamic and thermodynamic properties should be taken into account for studies of deep convection initiation and characteristics.

Acknowledgments. The authors are grateful to their colleagues from CRPE, EERM, LAMP and IOPG who participated in the experiments and provided many data used in this study. They also thank the reviewers for their comments and suggested language improvements. This work was supported by CNET and INSU.

REFERENCES

Asai, T., 1972: Thermal instability of a shear flow turning the direction with height. *J. Meteor. Soc. Japan,* **50,** 525–532.

Brown, R. A., 1972: On the inflection point instability of a stratified Ekman boundary layer. *J. Atmos. Sci.,* **29,** 850–859.

Brown, R. A., 1980: Longitudinal instabilities and secondary flows in the planetary boundary layer. A review. *Rev. Geophys. Space Phys.,* **18,** 683–697.

Caughey, S. J., and S. G. Palmer, 1979: Some aspects of turbulence structure through the depth of the convective boundary layer. *Quart. J. R. Meteor. Soc.,* **105,** 811–827.

Chong, M., and J. Testud, 1983: Three dimensional wind field analysis from dual Doppler radar data. Part 3: The boundary condition: an optimum determination based on a variational concept. *J. Climate Appl. Meteor.,* **22,** 1227–1241.

——, —— and F. Roux, 1983: Three dimensional wind field analysis from dual Doppler radar data. Part 2: Minimizing the error due to temporal variation. *J. Climate Appl. Meteor.,* **22,** 1216–1226.

Detman, T. R., and R. A. Kropfli, 1980: Doppler radar measurements in the PBL from Doppler radar. *Preprints, 19th Conf. on Radar Meteorology,* Miami, Amer. Meteor. Soc.

Doviak, R. J., and M. Berger, 1980: Turbulence and waves in the optically clear planetary boundary layer resolved by dual Doppler radars. *Radio Sci.,* **15,** 297–317.

Eymard, L., 1984: Radar analysis of a tropical convective boundary layer with shallow cumulus clouds. *J. Atmos. Sci.,* **41,** 1380–1393.

——, 1985: Convective organization in a tropical boundary layer: An interpretation of Doppler radar observations using Asai's model. *J. Atmos. Sci.,* **42,** 2844–2855.

——, and A. Weill, 1982: Investigation of clear air convective structures in the PBL using a dual Doppler radar and Doppler sodar. *J. Appl. Meteor.,* **21,** 1891–1906.

Frisch, A. S., R. B. Chadwick, W. R. Moninger and J. M. Young, 1976: Observation of boundary layer convection cells measured by dual Doppler radar and echosonde and by microbarograph array. *Bound. Layer Meteor.,* **10,** 55–68.

Hardy, K. R., and H. Ottersten, 1969: Radar investigations of convective patterns in the clear air atmosphere. *J. Atmos. Sci.,* **26,** 666–672.

Jensen, N. O., and D. M. Lenshow, 1978: An observational investigation of penetrative convection. *J. Atmos. Sci.,* **35,** 1924–1933.

Kaimal, J. C., J. C. Wyngaard, D. A. Haugen, O. R. Cote, Y. Izumi, S. J. Caughey and C. J. Readings, 1976: Turbulence structure in the convective boundary layer. *J. Atmos. Sci.,* **33,** 2152–2169.

——, R. A. Eversole, D. H. Lenshow, R. B. Stankov, P. H. Kahn and J. A. Businger, 1982: Spectral characteristics of the convective boundary layer over uneven terrain. *J. Atmos. Sci.,* **39,** 1098–1114.

Kelly, R. D., 1982: A simple Doppler radar study of horizontal roll convection in a lake-effect snow storm. *J. Atmos. Sci.,* **39,** 1521–1531.

——, 1984: Horizontal roll and boundary layer interrelationships observed over Lake Michigan. *J. Atmos. Sci.,* **41,** 1816–1826.

Kitchen, M., and S. J. Caughey, 1981: Tethered balloon observations of the structure of small cumulus clouds. *Quart. J. Roy. Soc.,* **107,** 853–874.

——, J. R. Leighton and S. J. Caughey, 1983: Three case studies of shallow convection using a tethered balloon. *Bound.-Layer Meteor.,* **27,** 282–308.

Konrad, T. G., 1970: The dynamics of the convective process in the clear air as seen by radar. *J. Atmos. Sci.,* **27,** 1138–1147.

Kropfli, R. A., and N. M. Kohn, 1978: Persistent horizontal rolls in the urban mixed layer as revealed by dual Doppler radar. *J. Appl. Meteor.,* **17,** 671–676.

——, and P. H. Hildebrand, 1980: Doppler radar measurements in the PBL during PHOENIX. *Preprints, 19th Conf. on Radar Meteorology,* Miami, Amer. Meteor. Soc.

Kuettner, J., 1971: Cloud bands in the earth's atmosphere: Observations and theory. *Tellus* **23,** 404–425.

Lemone, M. A., 1973: The structure and dynamics of horizontal roll vortices in the planetary boundary layer. *J. Atmos. Sci.,* **30,** 1077–1091.

——, 1976: Modulation of turbulence energy by longitudinal rolls vortices in the PBL. *J. Atmos. Sci.,* **30,** 1077–1091.

Lenshow, D. H., J. C. Wyngaard and W. T. Pennell, 1980: Mean-field and second moment budgets in a baroclinic, convective boundary layer. *J. Atmos. Sci.,* **37,** 1313–1326.

Miller and Strauch, 1974: A dual Doppler radar method for the determination of wind velocities within precipitating weather systems. *Remote Sens. Environ.* **3,** 219–235.

Nicholls, S., and M. A. Lemone, 1980: The fair weather boundary layer in GATE: The relationship of subcloud fluxes and structure to the distribution and enhancement of cumulus clouds. *J. Atmos. Sci.,* **37,** 2051–2067.

Unauthenticated | Downloaded 09/26/22 10:29 AM UTC

Nutten, B., P. Amayenc, M. Chong, D. Hauser, F. Roux and J. Testud, 1979: The RONSARD radars: A versatile C-band dual Doppler facility. *IEEE Trans. Geosci. Electron.*, **GE17,** 281–288.

Olesen, M. R., S. E. Larsen and J. Hojstrup, 1984: Modelling velocity spectra in the lower part of the planetary boundary layer. *Bound.-Layer Meteor.*, **29,** 285–312.

Pennell, W. T., and A. Lemone, 1974: An experimental study of turbulence structures in the fair weather trade wind boundary layer. *J. Atmos. Sci.*, **31,** 1308–1323.

Rabin, R. M., R. J. Doviak and A. Sundara-Rajan, 1982: Doppler radar observations of momentum flux in a cloudless convective layer with rolls. *J. Atmos. Sci.*, **39,** 851–863.

Reinking, R. F., R. J. Doviak and G. O. Gilmer, 1981: Clear air roll vortices and turbulent motions as detected with an airborne gust probe and dual Doppler radar. *J. Appl. Meteor.*, **20,** 678–685.

Sommeria, G., and J. Testud, 1984: "COPT 81": A field experiment designed for the study of dynamic and electrical activity of deep convection in continental tropical regions. *Bull. Amer. Meteor. Soc.*, **65,** 4–10.

Stull, R. B., 1976: Internal gravity waves generated by penetrative convection. *J. Atmos. Sci.*, **33,** 1279–1280.

Testud, J., and M. Chong, 1983: Three dimensional wind field analysis from dual Doppler radar. Part I: Filtering interpolating and differentiating the raw data. *J. Climate Appl. Meteor.*, **22,** 1204–1215.

Turner, J. S., 1973: Buoyancy effects in fluids, Cambridge University Press, 367 pp.

Weill, A., C. Klapisz, B. Strauss, F. Baudin, C. Jaupart, P. Van Grunderbeeck and J. P. Goutorbe, 1980: Measuring heat flux and structure functions of temperature fluctuations with an acoustic Doppler sodar. *J. Appl. Meteor.*, **19,** 199–205.

Wyngaard, J. C., 1981: Boundary layer modeling. Atmospheric turbulence and air pollution, F. T. M. Nieuwstadt and H. Van Dop, Eds., D. Reidel, 358 pp.

Unauthenticated | Downloaded 09/26/22 10:29 AM UTC